atmosphere

MDPI

Article

Seasonal Distribution and Source Apportionment of Chemical Compositions in $PM_{2.5}$ in Nanchang, Inland Area of East China

Hong Huang [1], Xin Yin [1], Yuan Tang [1], Changwei Zou [1,*], Jianlong Li [1], Chenglong Yu [2] and Fangxu Zhu [3]

[1] Key Laboratory of Poyang Lake Environment and Resource Utilization, Ministry of Education, School of Resources & Environment, Nanchang University, Nanchang 330031, China; honghuang@ncu.edu.cn (H.H.); 415800210056@email.ncu.edu.cn (X.Y.); 5811121047@email.ncu.edu.cn (Y.T.); jlli@ncu.edu.cn (J.L.)

[2] School of Land Resources and Environment, Jiangxi Agricultural University, Nanchang 330045, China; hjclyu@jxau.edu.cn

[3] No. 270 Research Institute of Nuclear Industry, Nanchang 330200, China; zhufangxu@cnuc.cn

* Correspondence: cwzou@ncu.edu.cn

Abstract: $PM_{2.5}$ was sampled in four seasons of 2021 in Nanchang. Organic carbon (OC), elemental carbon (EC), and water-soluble ions were the main chemical compositions in $PM_{2.5}$. The annual average of OC/$PM_{2.5}$ and EC/$PM_{2.5}$ was 17.1% and 2.1%, respectively, while nine water-soluble ions were 56.7%. The order of each ion percentage in $PM_{2.5}$ was NO_3^- > SO_4^{2-} > K^+ > Na^+ > NH_4^+ > Cl^- > NO_2^- > Ca^{2+} > Mg^{2+}. The OC/EC (6.54, 13.17, 8.95, 7.99) and Char-EC/Soot-EC (0.88, 0.64, 1.32, 3.74) indicated that the carbon aerosols mainly originated from coal combustion, biomass combustion, and motor-vehicle emissions. High concentrations of Cl^- and Ca^{2+} in spring were associated with dust sources. A good correlation between Na^+, SO_4^{2-}, and NO_3^- suggests the formation of Na_2SO_4 and $NaNO_3$. The results of $PM_{2.5}$ source apportionment by positive matrix factorisation (PMF) showed five main sources: motor-vehicle sources (18–33%), secondary sources (16–36%), coal combustion sources (16–30%), biomass-combustion sources (10–28%), and dust sources (5–7%). Backward trajectory clustering analysis showed $PM_{2.5}$ in spring and autumn were more influenced by medium distance and local air but mainly influenced by local sources in winter.

Keywords: $PM_{2.5}$; OC; EC; water-soluble ions; source apportionment

check for updates

Citation: Huang, H.; Yin, X.; Tang, Y.; Zou, C.; Li, J.; Yu, C.; Zhu, F. Seasonal Distribution and Source Apportionment of Chemical Compositions in $PM_{2.5}$ in Nanchang, Inland Area of East China. *Atmosphere* **2023**, *14*, 1172. https://doi.org/10.3390/atmos14071172

Academic Editor: Matteo Rinaldi

Received: 30 May 2023
Revised: 11 July 2023
Accepted: 11 July 2023
Published: 20 July 2023

1. Introduction

$PM_{2.5}$ and some of their chemical compositions have effects on solar radiative forcing [1,2], which affects the environment and climate adversely and are hazardous to human health due to the carcinogens and teratogens in $PM_{2.5}$. Carbonaceous aerosols are an important component of $PM_{2.5}$, mainly organic carbon (OC), elemental carbon (EC) and carbonate carbon (CC) [3,4]. Ji [5] studied the concentration levels and sources of carbon fractions in $PM_{2.5}$ in Handan and their variation patterns and determined that the mass concentration of the carbon fractions in $PM_{2.5}$ are high in autumn and winter and low in spring and summer; its sources were mainly biomass combustion, coal combustion emissions, and diesel-vehicle exhaust. Srinivas [6] collected $PM_{2.5}$ samples in the Ganges Plain region and analysed their carbon fraction and the presence of secondary production of OCs. Water-soluble inorganic ions are also an important chemical component of $PM_{2.5}$, mainly SO_4^{2-}, NO_3^-, NH_4^+, Na^+, Ca^{2+}, Cl^-, K^+, and Mg^{2+} [7]. Regarding foreign studies, Katarzyna [8] collected $PM_{2.5}$ in the Polish region throughout 2016 and showed that NO_3^- and secondary organic carbons (SOCs) dominated $PM_{2.5}$ and that there were differences in seasonal variation between the different components. Liu [9] observed $PM_{2.5}$ and its chemical components in the Taiyuan region and concluded that SO_4^{2-}, NO_3^-, NH_4^+, and Cl^- were the main chemical components of $PM_{2.5}$ and that coal-fired sources contributed more to the atmospheric $PM_{2.5}$ in the region.

The sources of $PM_{2.5}$ were complex and diverse and the distribution characteristics were varied in different regions [10]. It is important to study the chemical composition of $PM_{2.5}$ and quantitatively analyse its sources for regional air-pollution prevention and control. For the source analysis of carbonaceous aerosols, the main methods are ratio analysis, principal component analysis (PCA), positive matrix factorisation (PMF), and backward trajectory and potential source analysis. The ratio-analysis method can identify the main sources of carbonaceous aerosols. The PCA and PMF analyses allow quantification of the contribution of various potential sources to the concentration of carbon aerosols, while the backward trajectory method was mainly used to determine the influence of external transport on carbon aerosols [5]. Shen [11] used PCA and backward trajectory for source analysis in Beijing. The results showed that secondary pollution is more serious in summer, and the main sources of carbon aerosols are mixed motor-vehicle emissions, road dust, and combustion sources. Zhang [12] determined that the order of carbon fraction content and EC_1 was higher in winter in Harbin, which indicated that coal combustion and vehicle exhaust were the main sources of air pollution, and the contribution of biomass-combustion sources increased in winter. Li [13] used PCA to analyse the eight carbon components of PM_{10} in Shenyang and concluded that the main sources of OC and EC were vehicle-exhaust sources and fossil-fuel combustion sources. In recent years, studies on the spatial and temporal distribution characteristics and source apportionment of $PM_{2.5}$ and its chemical components have been a hot topic in the field of atmospheric science [14].

Nanchang, the capital city of the Jiangxi Province in the inland area of East China and one of the central cities in the middle and lower regions of the Yangtze River, is located in the subtropical humid monsoon climate zone with a humid and mild climate, high precipitation, strong solar radiation, active atmospheric photochemical reactions, and high frequency of acid rain [15]. Recently, with the rapid development of industry, energy consumption, fossil-fuel combustion, and the number of motor vehicles have been increasing. The situation of air quality deserves attention. We have carried out some previous studies on the chemical composition and source of $PM_{2.5}$ in Nanchang and obtained some results [16]; however, with the gradual expansion of the Nanchang urban area, especially the rapid development of Honggutan district, it is still necessary to further study the distribution characteristics and source apportionment of $PM_{2.5}$ in this region.

In this paper, $PM_{2.5}$ in the atmosphere of Nanchang was focused on, and $PM_{2.5}$ was sampled in the four seasons during March–December 2021. The carbon components and water-soluble ions in $PM_{2.5}$ were determined by carbon analyser and ion chromatography, respectively [17]. The distribution characteristics and influencing factors of $PM_{2.5}$, its carbon components, and water-soluble ions were analysed. Based on the distribution characteristics, two source apportionment methods/models (PMF and backward trajectory clustering analysis) were applied to further identify the sources of $PM_{2.5}$. It is meaningful to scientifically assess and prevent and control the effects and hazards of $PM_{2.5}$, which provide a scientific basis and data support for further prevention and control of particulate pollution in this study region.

2. Materials and Methods

2.1. Sample Collection

The sampling site (115°47′33″ E, 28°39′47″ N) was located in Nanchang City, in the inland area of East China, about 25 m above ground level with no typical industrial pollution sources nearby and no natural or artificial objects higher than the sampling site within 500 m. It was a mixed receptor site influenced by a mixture of road-traffic exhaust, industrial and domestic emission sources, construction dust, and other urban sources.

From March to December 2021, $PM_{2.5}$ was collected using a MiniVol portable airborne particulate sampler (flow rate 5 L/min) with a British Whatman quartz fibre filter (diameter 47 mm) for three consecutive days per month, with a collection time of 24 h for each sample. Before sampling, the filter membranes were pre-treated by wrapping them in aluminium foil and placing them in a muffle furnace (at 500 °C) for 6 h. After drying, the membrane is

placed in a transparent shell, washed with distilled water, placed together in a drying dish at constant temperature and humidity for 24 h, and then stored in a freezer for sampling.

2.2. Determination of $PM_{2.5}$ and Its Chemical Components

$PM_{2.5}$ mass concentration was determined by the weight method. The determination of OC and EC in $PM_{2.5}$ was performed using a DRI2015 thermo-optical carbon analyser [18] and the pyrolysis warming process was set to gradient warming to determine the eight carbon fractions of OC_1, OC_2, OC_3, OC_4, EC_1, EC_2, EC_3, and optical pyrolysed carbon (OPC). The pyrolysis process is based on the IMPROVE A procedure.

The thermal-optical carbon analysis [19] is based on the different order of oxidation of OC and EC at different temperatures and atmospheres. The function relies on the fact that organic compounds can be volatilised from the sample membrane in a nonoxidising helium (He) environment, whereas EC must be burned with the oxidising agent. In an oxygen-free pure helium environment, the OC on the sample filter is released by four pyrolysis passes. The pyrolysis ramp-up process is set to a gradient of 70–100 °C at a time with a final ramp-up to 900 °C. During this ramp-up process, the eight carbon fractions OC_1–OC_4, EC_1–EC_3, and OPC are measured separately. OC_1, OC_2, OC_3, and OC_4 are the carbons produced from atmospheric conditions (−25 °C) to 140 °C, 140 °C to 280 °C, 280 °C to 480 °C, and 480 °C to 580 °C in the presence of He, respectively; OPC is the carbon produced by returning the reflected or transmitted light from the laser measurement filter to its initial value in the presence of 98% He and 2% O_2 at a temperature of 580 °C. EC_1, EC_2, EC_3, and EC_4 are the carbons produced at 580 °C, 580–740 °C, and 740–840 °C in the presence of 98% He and 98% HeO_2, respectively. The principle is that the carbon-containing material in the membrane is pyrolysed to produce CO_2, then the CO_2 is converted to CH_4 by a catalyst (MnO_2), and the carbon content is converted by the CH_4 detected by a hydrogen flame ionisation detector (FID). The content of OC is equal to the sum of the masses of OC_1, OC_2, OC_3, OC_4, and OPC, while the content of EC is equal to the sum of the masses of EC_1, EC_2, and EC_3 minus the mass of OPC. These values are explained by Equations (1) and (2):

$$OC = OC_1 + OC_2 + OC_3 + OC_4 + OPC \quad (1)$$

$$EC = EC_1 + EC_2 + EC_3 - OPC \quad (2)$$

Half of the filter sample was cut with ceramic scissors and placed in an ultrasonic cleaner with ice water for 1 h. The sample was filtered with a disposable syringe and transferred to a clean centrifuge tube for testing. The water-soluble inorganic cations (Na^+, NH_4^+, K^+, Mg^{2+}, Ca^{2+}) in an ultrapure water extract of $PM_{2.5}$ were determined by ICS-1100 (Dionex Inc., Sunnyvale, CA, USA) ion chromatography with a CS12A column, CG12A guard column, and ASRS-300 suppressor, using 20 mmol/L methane sulfonic acid as the eluent. The water-soluble inorganic anions (Cl^-, NO_2^-, NO_3^-, SO_4^{2-}) in an ultrapure water extract of $PM_{2.5}$ were determined by ICS-5000 + SP (Dionex Inc., USA) with an AS18 column, AG18 guard column, and ASRS-300 suppressor, using a 40 mmol/L NaOH solution with a flow rate of 1.0 mL/min.

2.3. Date of Meteorological Factors

Meteorological factors were observed by weather stations installed beside the $PM_{2.5}$ sampling site. Rainfall amount, rainfall intensity, and atmospheric visibility were obtained from OTT laser raindrop spectra installed beside the $PM_{2.5}$ sampling site.

3. Results and Discussion

3.1. Distribution Characteristics of Different Components of $PM_{2.5}$

3.1.1. Proportion of Components of $PM_{2.5}$ and Its Seasonal Distribution

Figure 1 shows the proportions of OC, EC, and water-soluble ions in $PM_{2.5}$ of this study. The average proportion of OC in $PM_{2.5}$ in the four seasons ranged from 13.2% to 18.9% and the annual average proportion was 17.1%. The average proportion of EC in

$PM_{2.5}$ in the four seasons ranged from 1.7% to 2.5%, with a mean of 2.1%. The average annual proportion of total carbon (TC) to $PM_{2.5}$ was 19.2%, indicating that OC and EC were important components of $PM_{2.5}$.

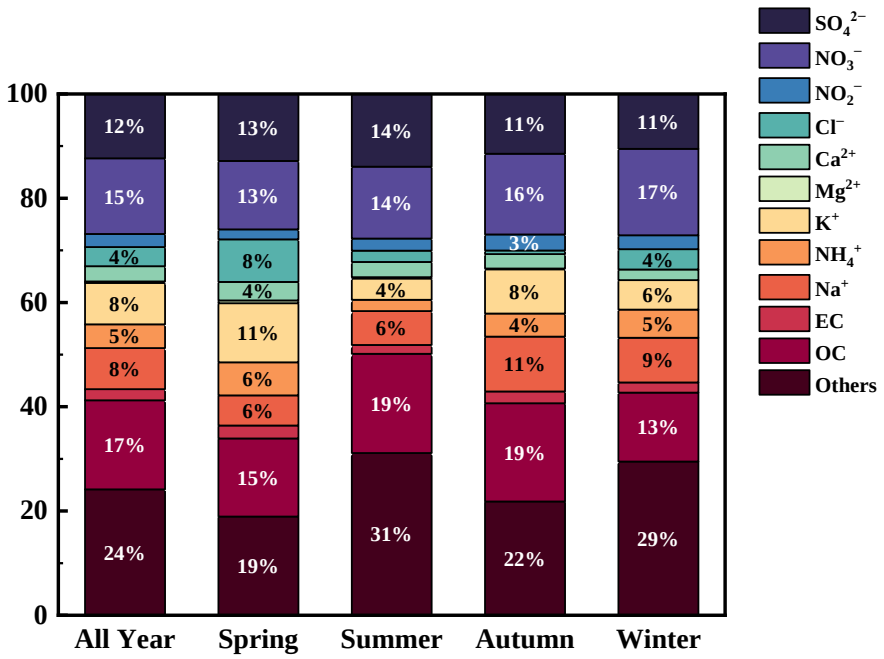

Figure 1. Distribution of OC, EC, and water-soluble ions in $PM_{2.5}$ during the sampling period throughout the year and in spring, summer, autumn, and winter.

The variation of OC/$PM_{2.5}$ in different seasons was greater than that of EC/$PM_{2.5}$. Since part of OC is volatile organic compounds, under some conditions this part of OC may volatilise. Differences in seasonal meteorological conditions (such as temperature, humidity, etc.) lead to differences in the gas–solid distribution of semivolatile organic compounds [20]. EC is inert, non-volatile, and difficult to decompose. The above were all the reasons why OC/$PM_{2.5}$ fluctuated more than EC/$PM_{2.5}$ did.

The results showed that OC/$PM_{2.5}$ and EC/$PM_{2.5}$ in winter were not the highest of the four seasons, although the concentrations of OC and EC were the highest in winter. It indicated that the primary emission sources in winter contributed more to the inorganic components in $PM_{2.5}$ but less to the carbon components compared with other seasons. In addition, the proportions of OC in $PM_{2.5}$ in summer and autumn (19% and 18.9%, respectively) were significantly higher than those in spring and winter (15% and 13.2%, respectively), reflecting the meteorological conditions. High temperature and humidity in summer and high temperature in autumn were conducive to the formation of secondary organic aerosols, which increased the proportion of OC in $PM_{2.5}$ in summer and autumn.

The proportion of the nine water-soluble ions in $PM_{2.5}$ was 56.7% throughout the year, and 63.6%, 48.2%, 57%, and 55.3% in spring, summer, autumn, and winter, respectively, indicating that water-soluble ions were the most important chemical components in $PM_{2.5}$ in the study area. The order of annual average proportion of water-soluble ions in $PM_{2.5}$ was: $NO_3^- > SO_4^{2-} > K^+ > Na^+ > NH_4^+ > Cl^- > NO_2^- > Ca^{2+} > Mg^{2+}$.

NO_3^-, SO_4^{2-}, K^+, Na^+, and NH_4^+ accounted for 83.4% of the total water-soluble ions. The secondary ions NO_3^-, SO_4^{2-}, and NH_4^+ (collectively referred to as secondary inorganic aerosol; SNA) accounted for 55.6% of the total water-soluble ions, indicating that SNA were the important components of water-soluble inorganic ions in $PM_{2.5}$, and $PM_{2.5}$ in this area was greatly affected by anthropogenic sources.

The proportion of NO_3^- was the highest (the annual average = 14.5%; 13.1%, 13.8%, 15.5%, and 16.6% in spring, summer, autumn, and winter, respectively), which was attributed to the fact that the primary source emitted more NO_2, and NO_2 generated more

NO_3^- after a photochemical reaction. The seasonal difference of the NO_3^- proportion in $PM_{2.5}$ (higher in winter than in summer) was attributed to the fact that nitrate was easy to decompose in summer, while low temperatures in winter were not conducive to nitrate decomposition. SO_4^{2-} accounted for the second largest proportion (annual average = 12.4%; 12.8%, 13.9%, 11.4%, and 10.5% in spring, summer, autumn, and winter, respectively). The highest proportion of SO_4^{2-} in summer was attributed to the fact that the high temperature and strong radiation make SO_2 easier to be photochemically oxidised to SO_4^{2-}. NH_4^+ mainly came from the transformation of NH_3 in the atmosphere, including the neutralisation of NH_3 with acidic substances, such as SO_2 and NO_2, in the atmosphere. NH_4^+ was jointly affected by NO_3^- and SO_4^{2-}. The proportion of NH_4^+ was higher in spring and winter (6.3% and 5.4%, respectively) and the lowest in summer (2.2%). The main reason may be that the emissions of primary gaseous precursors increased in spring and winter; the meteorological conditions in winter were not conducive to the diffusion of atmospheric pollutants and ammonium salts were unstable and easy to decompose in summer. K^+ in $PM_{2.5}$ in the study area accounted for a relatively high proportion (annual average = 7.9%; 11.4%, 4.1%, 8.5%, and 5.6% in spring, summer, autumn, and winter, respectively), reflecting the contribution of biomass combustion to $PM_{2.5}$.

3.1.2. Distribution of OC and EC

Distribution of OC

Figure 2 shows the mass concentrations of OC and its fractions ($OC_{1–4}$, OPC) in $PM_{2.5}$ of Nanchang in the four seasons.

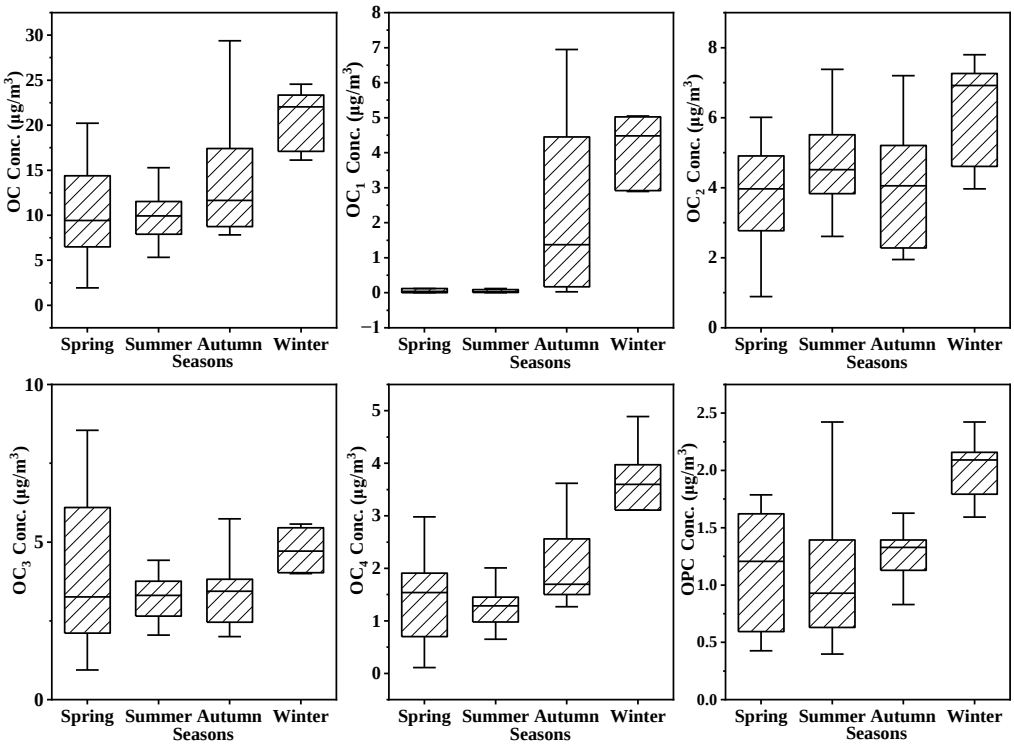

Figure 2. Seasonal distribution of OC and OC_1, OC_2, OC_3, OC_4, and OPC in $PM_{2.5}$ of Nanchang.

The concentrations of OC ranged from 1.9 to 31.1 μg·m^{-3} with a mean of 12.6 μg·m^{-3}. The highest OC concentration (30.08 μg·m^{-3}) occurred in November and the lowest (1.94 μg·m^{-3}) occurred in April.

The seasonal distribution of OC concentrations in Nanchang was characterised by a descending order of its concentration in winter (20.9 μg·m^{-3}), autumn (14.4 μg·m^{-3}), spring (10.6 μg·m^{-3}), and summer (10.2 μg·m^{-3}). The main fractions of OC were $OC_{1–4}$, accounting for about 84–95% of TOC, and their seasonal distribution of concentration

was characterised by a descending order of their concentration in winter (18.9 μg·m^{-3}), autumn (13.1 μg·m^{-3}), spring (9.6 μg·m^{-3}), and summer (9.5 μg·m^{-3}). OPC accounted for about 4–15% of TOC and its seasonal distribution was similar to that of OC, with the concentration in winter (2.0 μg·m^{-3}), autumn (1.3 μg·m^{-3}), spring (1.2 μg·m^{-3}), and summer (1.1 μg·m^{-3}) ranked in descending order.

The concentrations of OC, OC_{1-4}, and OPC were higher in winter and autumn than those in summer and spring, mainly due to lower temperatures and more emissions sources in winter, and increased vehicle start-up times in winter led to increased traffic emissions [21]. In addition, weaker solar radiation and weaker near-surface turbulence in winter promoted the continued accumulation of air pollutants and autumn was often the peak period of biomass-combustion emissions. Stable weather systems in autumn also facilitated pollutant accumulation. Relatively lower emissions intensity of pollution sources, strong solar radiation, and high wind speed in summer, together with frequent summer rainfall, were conducive to the diffusion and removal of pollutants in the atmosphere. Generally, high-temperature and humidity conditions in summer promote the formation of SOC. After carefully comparing the seasonal distribution of OC fractions and OC in Figure 2, it was found that the seasonal distributions of OC_2 and OC_3 were different from that of OC, while the seasonal distributions of OC_1, OC_4, and OPC were the same as that of OC. The concentration difference of OC_2 and OC_3 between summer and winter was not as large as that of OC between summer and winter, indicating that OC_2 and OC_3 were the main fractions of SOC.

Distribution of EC

Figure 3 shows the mass concentration distribution of EC, Char-EC (Char-EC = EC_1 − OPC), and Soot-EC (Soot-EC = EC_2 + EC_3).

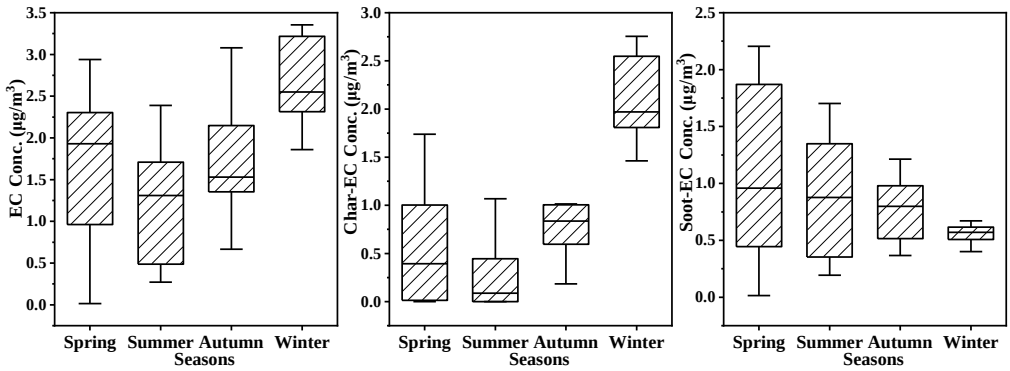

Figure 3. Seasonal distribution of EC, Char-EC, and Soot-EC in $PM_{2.5}$ of Nanchang.

The concentrations of EC ranged from 0.01 to 3.35 μg·m^{-3}, with a mean of 1.56 μg·m^{-3}. The highest EC concentration (3.35 μg·m^{-3}) occurred in December and the lowest (0.01 μg·m^{-3}) occurred in August. The seasonal distribution of EC concentrations in Nanchang was in a descending order in winter (2.6 μg·m^{-3}), autumn (1.7 μg·m^{-3}), spring (1.7 μg·m^{-3}), and summer (0.9 μg·m^{-3}). The seasonal distribution of Char-EC was in a descending order in winter (2.1 μg·m^{-3}), autumn (0.9 μg·m^{-3}), spring (0.6 μg·m^{-3}), and summer (0.1 μg·m^{-3}); the same as the seasonal distribution of EC, indicating that Char-EC was the main fraction of EC. The concentrations of EC and Char-EC were higher in winter and autumn than those in spring and summer, and their seasonal distribution characteristics were similar to that of OC, which was due to the combination of enhanced emissions of pollution sources and the static meteorological conditions in winter and autumn that favoured the accumulation of air pollutants. Different from the seasonal distribution characteristics of EC and Char-EC, the average concentrations of Soot-EC in spring, summer, and autumn were almost the same. In winter, Soot-EC was not as much higher than that of the other seasons as EC and Char-EC but lower than that of the other three seasons, reflecting that the emission

source of Soot-EC was relatively stable in different seasons. In addition, Soot-EC is a particulate carbon fraction formed by organic solids or liquids through gas-particle phase transformation at a high temperature (>600 °C) [22]. Low-temperature conditions in winter were not conducive to the generation and emission of Soot-EC, which was also the reason for the lower concentration of Soot-EC in winter.

Comparison of OC and EC in This Study with Those in Other Cities

Table 1 shows the concentrations of OC and EC in $PM_{2.5}$ in Nanchang and other cities around the world, where the sampling of $PM_{2.5}$ lasted for one year or nearly one year.

Table 1. Comparison of OC and EC in this study with those in other cities at home and abroad.

Sampling Site	Sampling Time	OC (μg·m^{-3})	EC (μg·m^{-3})	References
Nanchang	2021.3–2021.12	12.6	1.6	This study
Yangquan	2018.7–2019.3	8.0	3.6	[23]
Beijing	2017.12–2018.12	11.2	1.2	[24]
Guangzhou	2015.6–2016.05	8.2	1.8	[25]
Shenyang	2017.5–2017.8	9.6	2.3	[26]
Shanghai	2011.11–2012.12	10.7	2.0	[27]
Nanjing	2013.12–2014.10	18.0	6.7	[28]
Los Angeles, USA	2012.7–2013.6	4.5	1.4	[29]
Vanderbilt Park, South Africa	2009.3–2015.12	9.3	3.2	[30]
Toronto, Canada	2014.6–2017.4	1.2	0.7	[31]
Saitama Prefecture, Japan	2009.8–2010.4	5.5	3.3	[32]
Gwangju, Korea	2013.11–2014.11	4.1	1.5	[33]
Srinagar, India	2017.1–2017.12	15.3	5.2	[34]

The concentrations of carbon aerosol in Nanchang were at a moderate level compared with those in other cities listed in Table 1. Nanchang is a typical inland city and the sampling site was located in a densely populated area, close to the urban expressway (the nearest direct distance was about 100 m), representing the urban mixed receptor site. The source of particulate matter in the study area was complex and frequent human activities had significant effects on the emission and formation of carbon aerosols. The difference in OC and EC concentrations between Nanchang and other urban areas around the world also showed that the carbon components of $PM_{2.5}$ in this study were related to emission sources, the regional environment, and meteorological factors.

3.1.3. Distribution of SOC

Research showed a commonly used method for indirectly evaluating SOC in atmospheric particulate is the minimum OC/EC ratio method [11]. When the observed OC/EC reaches a minimum value, the SOC in the environment is largely negligible. The minimum OC/EC ratio method is simple compared to the minimum R-squared (RMS) method, but as pollutants enter the atmosphere further away from the emission source and undergo the ageing process, the minimum value of ρ(OC)/ρ(EC) observed is sometimes not a good representation of the $r(OC/EC)_{pri}$, resulting in a large difference between the actual SOC values; however, the MRS method is not a simple empirical assumption for calculating $r(OC/EC)_{pri}$, so the SOC calculated by the MRS method is closer to the actual value. In the study, the MRS method was used to determine the $r(OC/EC)_{pri}$ for each season. Figure 4 shows the estimated curve of $r(OC/EC)_{pri}$ in four seasons and Figure 5 shows the seasonal average values of SOC and primary organic carbon (POC). POCs are direct emissions, while SOCs are produced by photochemical reactions under favourable meteorological conditions [5].

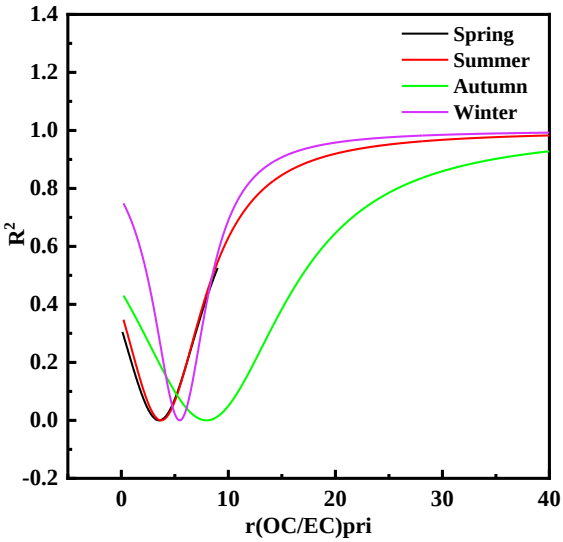

Figure 4. Relationship between the correlation coefficient R^2 of SOC and EC and the assumed $r(OC/EC)_{pri}$.

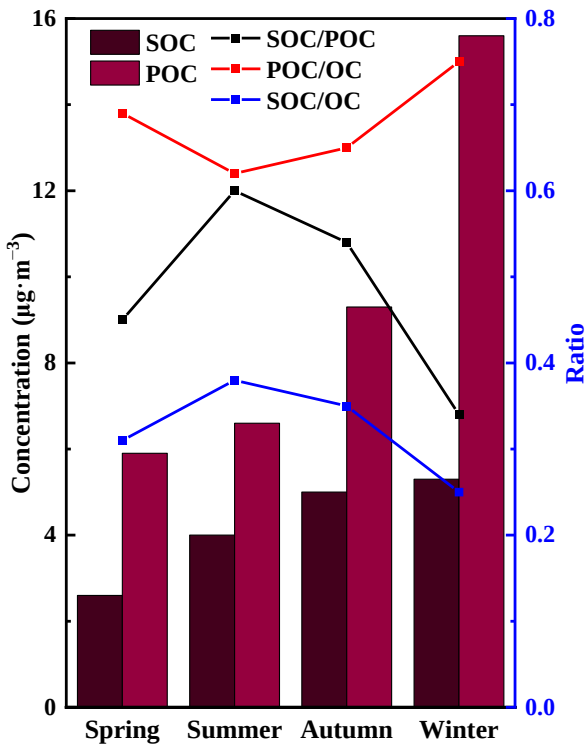

Figure 5. SOC, POC, and r(SOC/POC), r(POC/OC), and r(SOC/OC) seasonal averages.

The $r(OC/EC)_{pri}$ values fitted by the MRS method were 3.46, 6.96, 5.45, and 5.90 in spring, summer, autumn, and winter, respectively, when the correlation between SOC and EC was the weakest. The value of $r(OC/EC)_{pri}$ determined by the MRS method represented the ratio of OC/EC in the primary emission source of regional particulate matter. The OC/EC ratio was often used to judge the existence of SOC and to calculate SOC [35]. In this study, the $r(OC/EC)_{pri}$ value exceeded two in four seasons. Therefore, it was thought that the primary emission sources of regional particulate matter included a large part of the contribution of biomass-combustion sources. The OC/EC ratio of biomass-combustion sources is far greater than two, and the OC/EC ratio of primary emission sources of motor-vehicle exhaust and coal combustion is lower than two [36].

The seasonal distribution of SOC concentration was characterised by a descending order of its concentration in winter (5.3 μg·m^{-3}), autumn (5.0 μg·m^{-3}), summer (4.0 μg·m^{-3}), and spring (2.6 μg·m^{-3}). Higher concentrations of SOC in winter and autumn were mainly due to more primary emission sources in winter and autumn (including particulate POC and gaseous pollutants that will generate SOC under certain conditions). SOC/OC was the highest in summer (38%) and the lowest in winter (25%), reflecting that the higher relative humidity, higher temperature, and stronger solar radiation in summer provided favourable conditions for photochemical reactions, resulting in the easier oxidation of gaseous precursors (such as VOCs) to SOC.

3.1.4. Distribution of Eight Carbon Fractions

Figure 6 shows the proportions of the eight carbon fractions in total carbon (TC) throughout the year.

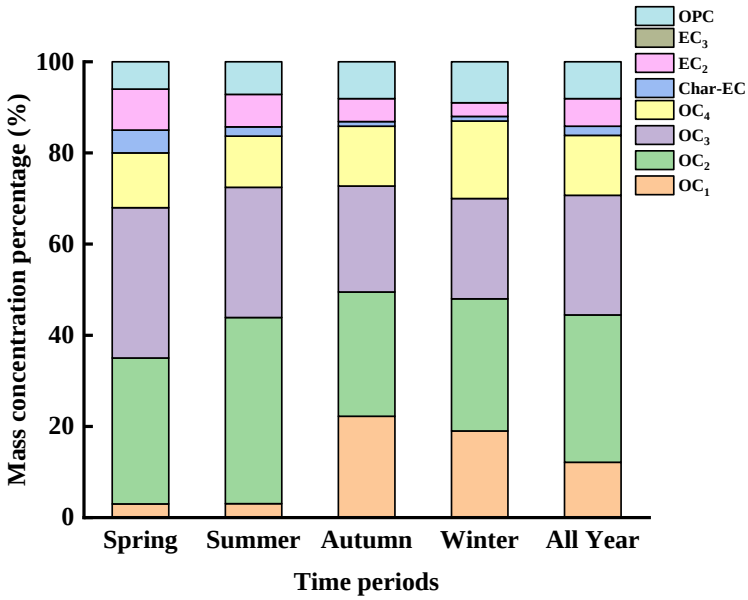

Figure 6. The proportion of eight carbon fractions in TC throughout the year and in four seasons.

The order of the annual average proportion of carbon fraction in TC was: OC_2 > OC_3 > OC_4 > OC_1 > OPC > EC_2 > Char-EC. The proportion of EC_3 in TC was approximately zero. According to Cao et al. [37], the contribution of aerosol pollution sources can be judged by the carbon fraction content. OC_1 has the highest content in biomass-combustion samples, OC_2, OC_3, OC_4, and EC_1 have higher content in coal-combustion emissions and motor-vehicle exhaust, and EC_2 and EC_3 have higher content in diesel-vehicle exhaust. The proportion of OC_2 was the highest proportion (30.91%) of the eight carbon fractions, indicating that coal combustion and motor-vehicle exhaust were important sources of carbon components in the atmosphere of Nanchang. The dominant carbon fractions in $PM_{2.5}$ in the study area were OC_1, OC_2, OC_3, OC_4, and EC_2, indicating that the main sources of regional carbon aerosols included coal combustion, biomass combustion, and gasoline and diesel-vehicle exhaust emissions. The seasonal distribution of the eight carbon fractions was different. The most obvious difference was that the ratios of OC_2 and OC_3 to TC in summer were significantly higher than that in winter. The high temperature and high humidity in summer were more conducive to the generation of SOC, reflecting that OC_2 and OC_3 were the main fractions of SOC.

3.1.5. Distribution of Water-Soluble Ions

Table 2 shows the annual average concentrations of water-soluble ions in $PM_{2.5}$ and those in four seasons.

Table 2. Concentrations of water-soluble ions in $PM_{2.5}$ (μg·m^{-3}).

Projects	Na^+	NH_4^+	K^+	Mg^{2+}	Ca^{2+}	Cl^-	NO_2^-	NO_3^-	SO_4^{2-}
Annual average	6.07	3.41	6.28	0.24	2.10	3.17	2.78	11.88	9.47
Spring	3.95	4.33	7.75	0.37	2.42	5.58	2.12	2.12	2.12
Summer	3.58	1.20	2.26	0.14	1.61	1.95	2.11	8.07	7.71
Autumn	8.29	3.37	6.47	0.19	2.09	2.34	3.25	14.17	10.59
Winter	14.04	7.40	8.64	-	2.67	7.20	4.20	25.62	13.64

For water-soluble anions, the seasonal distribution of NO_2^-, NO_3^-, and SO_4^{2-} concentrations were in a descending order in winter, autumn, summer, and spring, while the seasonal distribution characteristics of Cl^- were in a descending order in winter, spring, autumn, and summer. The lower concentration of NO_3^- in summer may be due to the fact that NO_3^- in the form of ammonium nitrate was more volatile when the temperature was higher in summer. The highest concentration of SO_4^{2-} in winter was related to the increase of SO_2 emission caused by heavy coal burning in winter. Although the meteorological conditions, such as a stable boundary layer and low wind, in winter, were not conducive to the secondary conversion of SO_2 to SO_4^{2-}, the liquid phase reaction and sufficient sources of SO_2 may also lead to a large amount of SO_4^{2-} formation [38]. High Cl^- concentrations in winter may be influenced by coal emissions or biomass burning, while high Cl^- concentrations in spring may be associated with high winds and dust.

For water-soluble cations, NH_4^+ concentration was the highest in winter, mainly because the increase of coal burning in winter led to the increase of SO_2 emissions and the SO_2 reacted with NH_3 in the atmosphere to produce a large amount of $(NH_4)_2SO_4$. The lower temperature in winter helped to stabilise the volatile components in particulate matter, resulting in the highest concentration of NH_4^+ in winter. Ca^{2+} mainly came from soil, sand, and construction dust. The high concentration of Ca^{2+} in the spring of this study was related to the source of spring aeolian sand. The highest K^+ concentration in winter may be related to coal and biomass combustion.

3.2. Source Apportionment of $PM_{2.5}$

3.2.1. Source-Analysis Based on the Correlations between Chemical Compositions

Correlations between OC and EC

Figure 7 shows the correlation between OC and EC in different seasons. The source of $PM_{2.5}$ can be traced generally by the correlations between OC and EC [39].

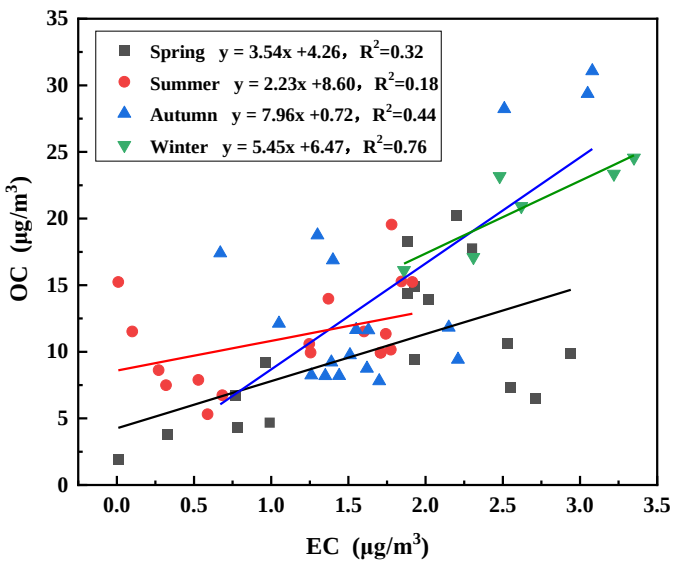

Figure 7. Correlation between OC and EC in four seasons.

A good correlation between OC and EC indicates that they share similar pollution sources and atmospheric diffusion processes and the poor correlation between OC and EC indicates the difference in sources, generally due to the secondary generation of SOC. The correlation coefficient of OC and EC was the highest in winter (R^2 = 0.76), indicating that most of the OC and all of the EC mainly originated from primary emission sources in winter. The correlation coefficient of OC and EC in summer was the weakest (R^2 = 0.18), indicating that the influence of secondary aerosols was the most prominent in summer.

Correlations between Water-Soluble Ions

By analysing the relationships between water-soluble ions in $PM_{2.5}$, their combinations and possible sources can be determined. The relationship of water-soluble ions over the whole year was shown in Figure 8.

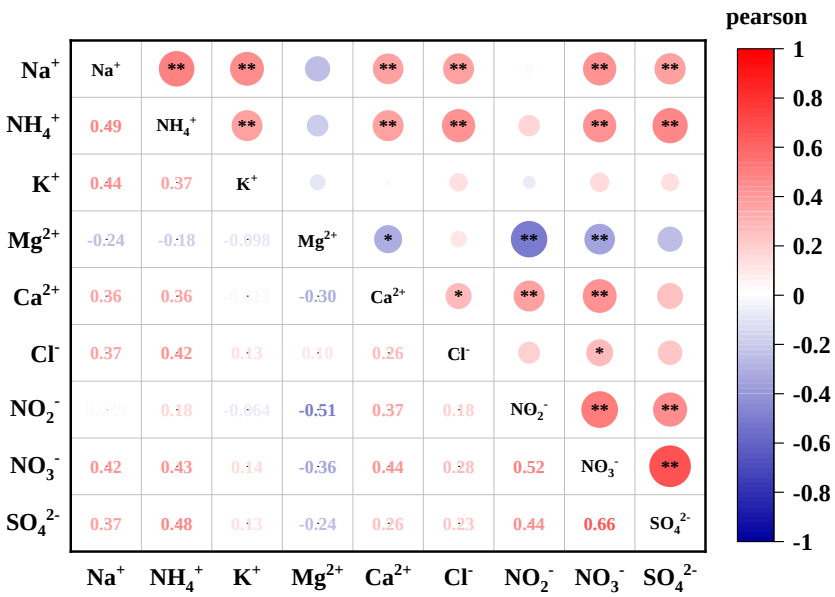

Figure 8. Relationship of water-soluble ions in $PM_{2.5}$ (* p <= 0.05, ** p <= 0.01).

The correlation coefficients between secondary ions NO_3^-, SO_4^{2-}, and NH_4^+ were 0.43–0.66 ($p \leq 0.01$), with good correlations, indicating the sources and production mechanisms of secondary ions had common parts and high similarity in their evolution and deposition in the atmosphere. SO_4^{2-} and NO_3^- showed an extremely significant positive correlation (R^2 = 0.66, $p \leq 0.01$), and SO_4^{2-} and NO_3^- were mainly derived from the photochemical transformation of gaseous precursors SO_2 and NO_2 released by fossil-fuel combustion. The strong correlation between SO_4^{2-} and NO_3^- indicated their homology, which meant that SO_4^{2-} and NO_3^- may be secondarily generated by the same gas-particle transformation mechanism. Among the correlations between NH_4^+ and other ions, the correlation coefficient with SO_4^{2-} was the highest (R^2 = 0.48, p < 0.01), followed by that with NO_3^- (R^2 = 0.44, $p \leq 0.01$). It was indicated that NH_4^+ combined most easily with SO_4^{2-} to form $(NH_4)_2SO_4$, followed by NO_3^- to form NH_4NO_3, and the reactivity of SO_4^{2-} was significantly higher than that of NO_3^-. SO_4^{2-} and NO_3^- in the water-soluble ions of $PM_{2.5}$ mainly exist in the form of $(NH_4)_2SO_4$ and NH_4NO_3. $(NH_4)_2SO_4$ exists stably in the atmosphere once formed. It was also indicated that NH_3 was the main substance to neutralise H_2SO_4 and HNO_3.

Cl^- showed a good correlation with five cations, indicating that Cl^- was more likely to exist in various forms, such as potassium chloride (KCl), ammonium chloride (NH_4Cl), calcium chloride ($CaCl_2$), magnesium chloride ($MgCl_2$), etc. Ca^{2+} from soil sources and construction-dust markers showed a good correlation with Cl^- (R^2 = 0.26, $p \leq 0.05$), suggesting that Cl^- may be partially influenced by soil dust. Cl^- correlated relatively well with Na^+ (R^2 = 0.37, $p \leq 0.01$), indicating some homology between the two. Na^+ and Cl^-

are considered to be characteristic ions of marine origin, with the ocean contributing high concentrations of Na^+ and Cl^- in coastal areas; but here in an inland city, both may also come from combustion sources, such as fossil-fuel combustion or food-industry emissions.

Na^+ correlated well with SO_4^{2-} and NO_3^- (R^2 = 0.37 and 0.42, respectively; $p \leq 0.01$), and SO_4^{2-} and NO_3^- can react nonhomogeneously on the surface of particles to form more stable sulphates and nitrates with alkaline metal ions, such as Na_2SO_4 and $NaNO_3$. Na^+ and Ca^{2+} showed a weak correlation, suggesting that they may partly originate from urban-debris dust in the city or from a distant input source.

3.2.2. Source-Analysis Based on OC/EC, EC/TC, and Char/Soot

The OC/EC ratio was used to trace the source and emission characteristics of carbon aerosols. Previous studies have shown that the characteristic OC/EC ratio of motor-vehicle exhaust emissions is 1.0–4.2 [40], the characteristic OC/EC ratio of biomass-combustion sources is 16.8–40 [41], and the characteristic OC/EC ratio of coal combustion is 2.5–10.5 [40]. Figure 9a shows the ratios of OC/EC in this study. Average OC/EC ratios were 6.54, 13.17, 8.95, and 7.99 in spring, summer, autumn, and winter, respectively. The OC/EC ratio values in this study were between the characteristic OC/EC ratios of the above primary sources, suggesting that the source of carbonaceous aerosols during the sampling period was complex and was contributed to by multiple sources (coal and biomass combustion, vehicle exhaust, etc.). Moreover, the OC/EC ratios in summer and autumn were higher than that in spring and winter, which may be attributed to the fact that the high temperature and strong radiation in summer and autumn promoted the formation of SOC. Also, more biofuels are available in the autumn harvest season, which increased the burning of agricultural residues.

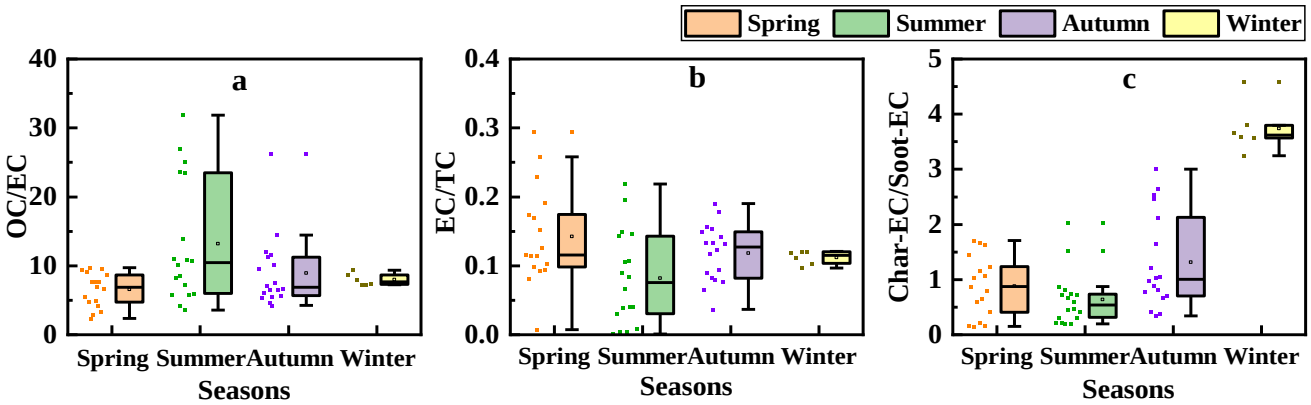

Figure 9. Seasonal distribution of (**a**) OC/EC, (**b**) EC/TC, and (**c**) Char-EC/Soot-EC in this study.

EC/TC ratios can be used to trace the sources of carbon-containing aerosols. The high EC/TC ratio indicates that the contribution of vehicle-exhaust emissions is large; on the contrary, the contribution of biomass combustion or SOC is small [39]. Figure 9b shows the ratios of EC/TC in this study. Average EC/TC ratios were 0.14, 0.08, 0.12, and 0.11 in spring, summer, autumn, and winter, respectively. In general, the vehicle emissions in the study area were relatively stable. The average values of EC/TC in spring, autumn, and winter were close but the lowest value of EC/TC in summer was not due to the reduction of vehicle-emission contributions in summer but to the increase of SOC in summer, which led to the increase of TC and the decrease of EC/TC ratio.

The Char-EC/Soot-EC ratio can also be used for the source tracing of carbon aerosols [42]. When Char-EC/Soot-EC < 1, the carbon aerosols are considered to be mainly from the vehicle exhaust and when it was greater than 3, carbon aerosols were considered to be mainly from biomass and coal combustion [43]. Figure 9c showed the ratios of Char-EC/Soot-EC in this study. Average Char-EC/Soot-EC ratios were 0.88, 0.64, 1.32, and 3.74 in spring, summer, autumn, and winter, respectively. The Char/Soot average was the

highest in winter (3.74), and the ratio was all greater than three for all samples, indicating that biomass combustion and coal combustion were the main contributors to EC in winter. The average value of Char/Soot in summer was less than one, and the Char/Soot of a small number of samples in summer was between one and three, reflecting that vehicle exhaust in summer was the main contributor to EC. The average values of Char/Soot in spring and autumn were slightly less than one, while half of the samples in spring and autumn were between one and three, reflecting that EC in spring and autumn consisted of motor-vehicle exhaust, biomass combustion, and coal combustion. The proportion of the Char/Soot ratio in autumn was slightly higher than that in spring, indicating that the contribution rate of biomass and coal combustion to EC in autumn was slightly higher than that in spring.

3.2.3. Source-Analysis Based on the PMF Method

PMF5.0 software was used to analyse the sources of the nine water-soluble ions and carbon components in $PM_{2.5}$ in Nanchang. The source composition spectrum of $PM_{2.5}$ resolved by PMF in four seasons is shown in Figure 10.

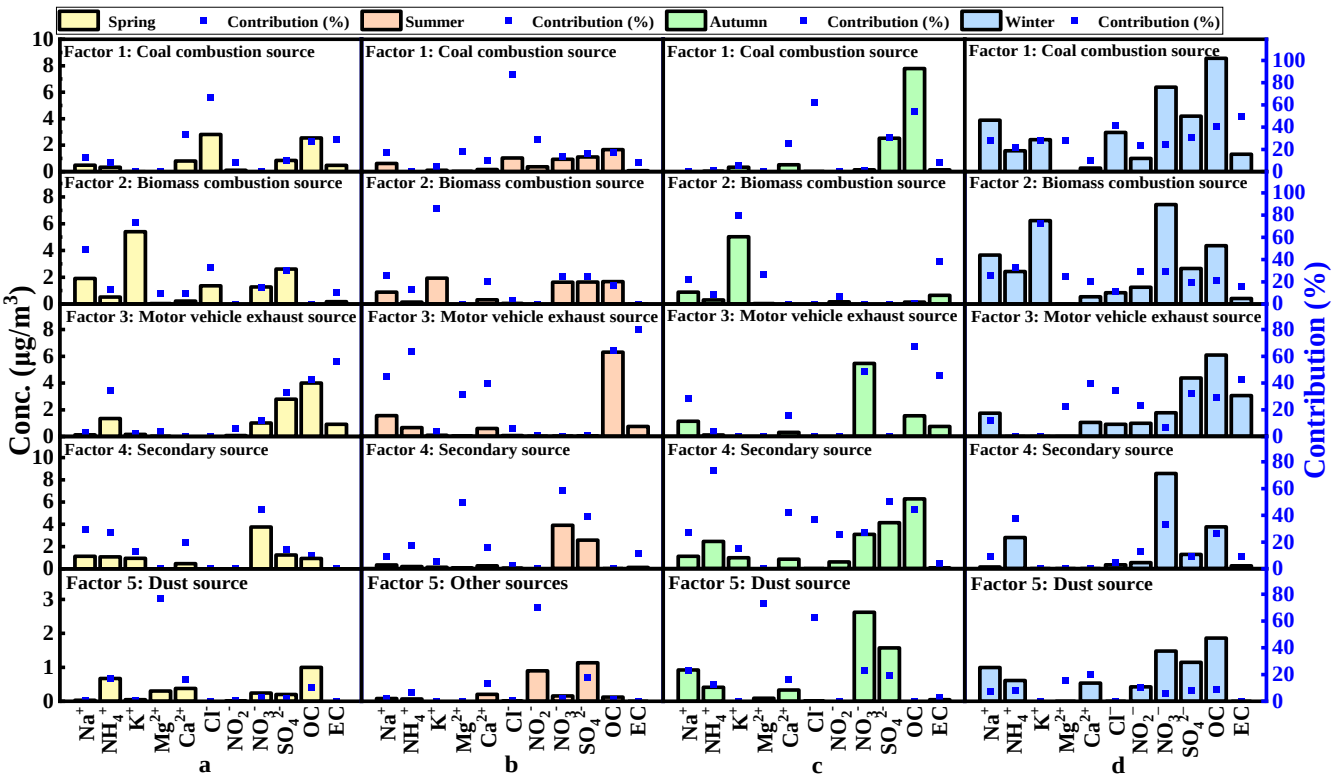

Figure 10. The component spectra by PMF model: (**a**) spring, (**b**) summer, (**c**) autumn, and (**d**) winter.

For the composition spectrum in four seasons by the PMF model, factor 1 shows the highest contribution of Cl^-, which is considered mainly from coal combustion in the area far from the sea [43]. Factor 2 shows a larger contribution of K^+, which is mainly from biomass combustion, so factor 2 can be judged to be a biomass-combustion source. Factor 3 shows the highest contribution of EC and OC, so factor 3 was thought to be a motor-vehicle exhaust source. Secondary ions NO_3^-, SO_4^{2-}, and NH_4^+ contributed prominently in factor 4, so factor 4 was considered as a secondary source. Factor 4 represented the secondary pollution formed by photochemical reactions of gaseous pollutants from fossil-fuel combustion (motor-vehicle fuel, etc.) and biomass-combustion activities in and around the sampling area. The source-analysis results showed that the contribution of factor 4 to $PM_{2.5}$ was highest in autumn, indicating that the weather conditions, such as a stable boundary layer and less rainfall, in autumn were more favourable to the formation of secondary pollution [44]. The increase of coal and biomass burning in winter stresses the

contribution of emissions from coal-fired and biomass-burning sources, which reduces the influence of secondary sources on the sampling area.

In the PMF figures of spring, autumn, and winter, factor 5 shows a large contribution of Mg^{2+} as a crustal element, which is consistent with the source-spectrum characteristics of soil dust, so factor 5 in the three seasons was identified as the source of dust. In the PMF figure in summer, there were obvious source-spectrum characteristics of soil dust, which may be related to the wet removal process of particles due to the heavy and frequent rainfall in summer. Factor 5 in summer shows prominent NO_2^- contribution and relatively average contributions of other components, so it is judged to be other sources mainly from industrial pollution. In summary, the main sources of $PM_{2.5}$ in the sampling area were coal-fired sources, biomass-combustion sources, motor-vehicle sources, secondary sources, and dust sources.

Based on the source-analysis results shown in Figure 11, it can be seen that the contribution of each source was relatively average in spring, with a stronger joint influence from biomass combustion and motor-vehicle emissions [45]. $PM_{2.5}$ in summer mainly came from motor-vehicle sources, which is consistent with the previous conclusion that meteorological conditions, such as high temperature and high humidity, in summer are favourable to the formation of secondary organic aerosols which increase the proportion of OC in $PM_{2.5}$. The contribution of secondary sources was prominent in autumn, while coal-fired sources and biomass-combustion sources contributed more in winter. The order of the annual contribution rate of each source throughout the year was the motor-vehicle source (23.25%), secondary source (23.25%), coal-combustion source (20.75%), biomass-combustion source (20.75%), and dust source (7.25%). The motor-vehicle source was the largest contributor, which was caused by the increasing number of motor vehicles in recent years. Coal-fired sources and biomass-combustion sources were the second main contributors, which were closely related to the surge in coal used for heating in winter and the existence of more biomass burning for heating and cooking activities in rural areas in winter.

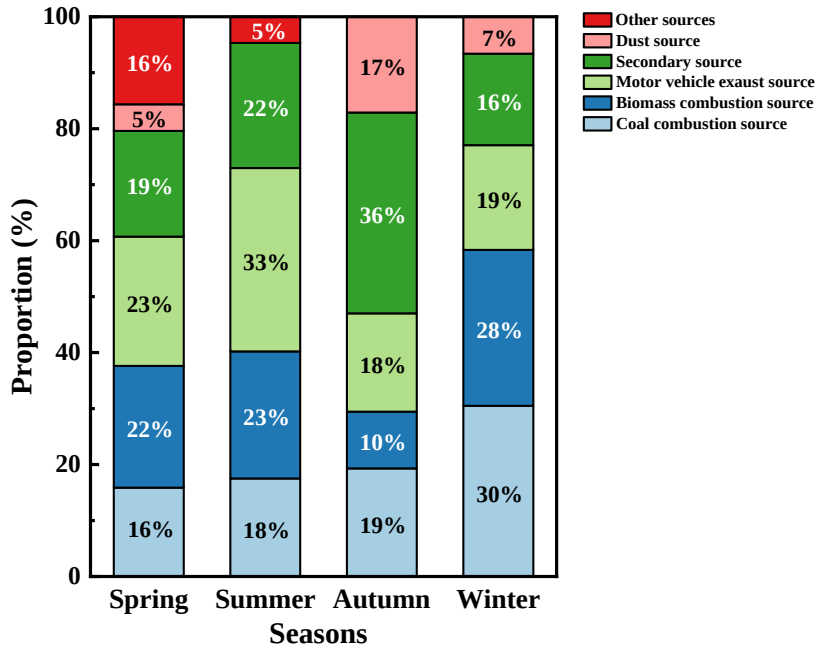

Figure 11. The source contribution rate by PMF model in four seasons.

3.2.4. Source Analysis Based on the Backward Trajectory Method

In order to study the sources of $PM_{2.5}$ in Nanchang, this study analyzed the atmospheric air-mass trajectories by the HYSPLIT backward trajectory model provided by NOAA, and the backward trajectory diagram is shown in Figure 12.

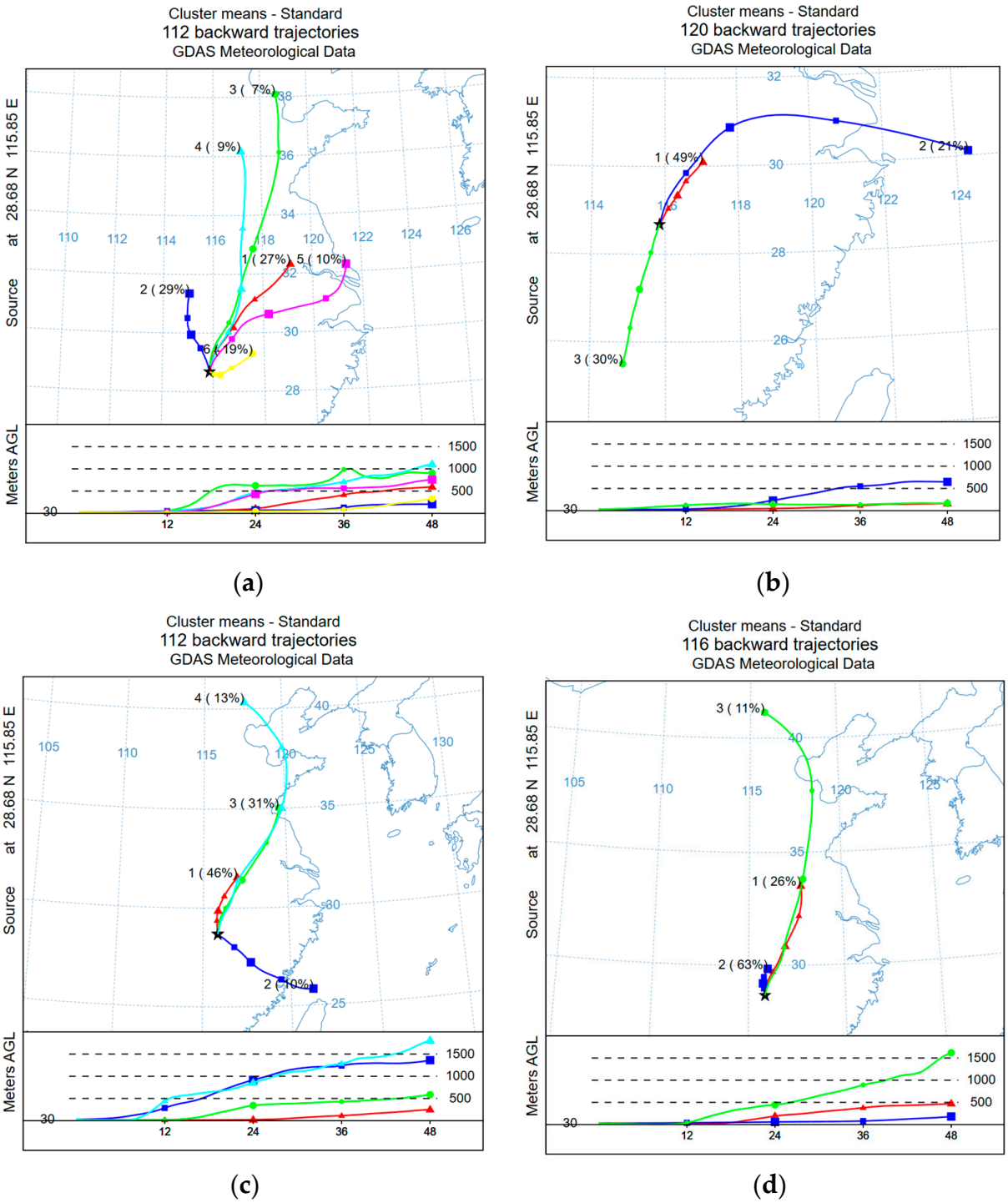

Figure 12. Backward trajectories diagrams for spring (**a**), summer (**b**), autumn (**c**), and winter (**d**).

In spring, the backward trajectory simulation for 48 h obtained a total of 112 backward trajectories. After cluster analysis, the number of clusters was set to six, based on the total spatial variance (TSV), which showed a scattered distribution of the clustered trajectories. Cluster 1, accounting for 27% of the total air masses, mainly came from southwest Jiangsu Province, which arrived at the sampling site southward through the interior of Anhui Province with an initial height of about 500 m. It was a low- to medium-altitude air mass that changed little in height during the movement, similar to cluster 2 with the largest proportion (29%) from Hubei. Clusters 3 and 4 were long-range transport air masses from Hebei and Shanxi, China, which may transport coal-fired and industrial pollutants but the

initial altitude of both masses was about 1000 m, belonging to the middle- and high-altitude air masses, with fast-moving speed and small proportions (7%, 9%). Cluster 5 accounted for 10% of the total air masses, from the south-eastern Jiangsu Province near the Yellow Sea region, and arrived at the study area via northeast Zhejiang Province. Cluster 5, cluster 1, and cluster 2 were medium-distance air masses with the greatest total share (66%), with airflow moving slowly in a curved path, easily causing the accumulation of pollutants. Cluster 6 was a local air mass accounting for 19%. In short, $PM_{2.5}$ in spring were mainly related to the accumulation of local pollution under static weather.

In summer, a total of 120 backward trajectories were obtained, and the cluster number was determined to be three according to the TSV. Cluster 1 came from the junction of Jiangxi and southwest Anhui Province, accounting for the largest proportion (49%), with a trajectory that was short, slow moving, at about 100 m high, and with a small horizontal span, which is prone to pollutant aggregation and short-distance transport. Cluster 2 came from the East China Sea region and was imported into the study area via Shanghai and Anhui. It was about 500 m high and belonged to the middle- and low-altitude air masses. Cluster 3 came from southern Guangdong, accounting for 30%, and showed the characteristics of close transport in the near stratum, similar to cluster 1.

In autumn, a total of 112 backward trajectories were obtained and the number of clusters was determined to be four based on the total spatial TSV. Cluster 1 came from the border between Jiangxi and Anhui, accounting for the largest share of 46%. The trajectory movement time was short and slow and many curves existed during the trajectory, which made it difficult for particulates to diffuse. Cluster 2 came from the East China Sea, was transported to the sampling site from the southeast via Fujian Province, and accounted for a relatively small percentage (10%). Cluster 3 came from the junction of Shandong and Jiangsu near the Yellow Sea area, indicating that the sampling area may be affected by marine sources in autumn. Cluster 4 came from the border between Hebei and Inner Mongolia and was transported to the sampling site via the Shandong and Anhui regions, similar to cluster 3. Both cluster 2 and cluster 4 originated at an altitude of about 1500 m, sinking and settling transport from the southeast and northeast directions, respectively, with faster air-mass movement.

In winter, a total of 116 backward trajectories were obtained and the number of clusters was determined to be three based on the TSV, with concentrated sources of trajectories. Cluster 1 was transported to the sampling area via Anhui Province, a medium-distance transported air mass, accounting for 26% of the total, with an initial height of 500 m. It was a low- to medium-altitude air mass that changed slightly in height during the movement. Cluster 2 was a local air mass with curved airflow and short trajectory, accounting for the largest proportion (63%), which is the main path of pollution transport, indicating that the sampling site has greater influence from local sources in winter. Cluster 3 was a high-altitude long-range air mass transported from the north of China, with the smallest proportion (11%), an initial height higher than 1,500 m, a long transmission distance, and a fast transmission speed.

4. Conclusions

The annual average for $OC/PM_{2.5}$ (17.1%) is higher than the annual average for $EC/PM_{2.5}$ (2.1%). Nine water-soluble ions make up the highest proportion of $PM_{2.5}$, with an annual average of 56.7%. The SNA accounted for 55.6% of the total water-soluble ions, indicating that $PM_{2.5}$ is influenced by some anthropogenic factors.

The annual average concentrations of OC and EC ranged from 1.9 to 31.1 $\mu g \cdot m^{-3}$ and from 0.01 to 3.35 $\mu g \cdot m^{-3}$, respectively. $r(OC/EC)_{pri}$ fitted by the MRS method exceeded two in all seasons, indicating that biomass combustion accounted for a large contribution. The order of average concentration of carbon fractions in TC was: $OC_2 > OC_3 > OC_4 > OC_1 >$ OPC $> EC_2 >$ Char-EC, indicating the contribution of coal combustion, biomass combustion, and vehicle-exhaust emissions. OC_2/TC and OC_3/TC were significantly higher in summer than in winter, indicating that OC_2 and OC_3 were the main components of SOC. SNA

concentrations were all highest in winter, related to the increasing coal combustion and weather conditions, while the high Cl^- and Ca^{2+} concentrations in spring may be related to winds and dust.

SNA correlations were 0.43–0.66 ($p \leq 0.01$), indicating the high similarity of sources, production, and evolution patterns. The OC-EC correlation was highest in winter (R^2 = 0.76), indicating that OC and EC mainly originated from primary emissions in winter. The OC/EC ratio (6.54, 13.17, 8.95, and 7.99) indicated carbonaceous aerosols were formed from multiple sources. The EC/TC (0.14, 0.08, 0.12, and 0.11) and Char-EC/Soot-EC ratios (0.88, 0.64, 1.32, and 3.74) indicated the main contributions to be coal combustion, biomass combustion, and motor-vehicle emissions. The results of PMF showed that motor-vehicle sources (23.25%), secondary sources (23.25%), coal-combustion sources (20.75%), biomass-combustion sources (20.75%), and dust sources (7.25%) were the main sources of $PM_{2.5}$. Backward trajectory analysis showed that $PM_{2.5}$ in spring and autumn were more influenced by medium distance and local air masses. In summer, $PM_{2.5}$ were mostly contributed to by near ground-level proximity transport, while in winter, they were mainly influenced by local sources.

Author Contributions: Conceptualization, H.H., X.Y. and C.Z.; software, X.Y. and Y.T.; validation, H.H., X.Y. and C.Z.; data curation, H.H. and X.Y.; writing—original draft preparation, H.H., X.Y. and C.Z.; writing—review and editing, H.H., X.Y., Y.T., C.Y., J.L. and F.Z.; supervision, H.H. and C.Z.; funding acquisition, H.H., J.L. and C.Y. All authors have read and agreed to the published version of the manuscript.

Funding: This work was supported by the National Natural Science Foundation of China (42265011, 52064037), the Natural Science Foundation of Jiangxi Province (20202BAB204030), and the Training Program for Academic and Technical Leaders of Major Disciplines in Jiangxi Province (20212BCJL23054).

Institutional Review Board Statement: Not applicable.

Informed Consent Statement: Not applicable.

Data Availability Statement: Not applicable.

Conflicts of Interest: The authors declare no conflict of interest. The funders had no role in the design of the study; in the collection, analyses, or interpretation of data; in the writing of the manuscript, or in the decision to publish the results.

References

1. Zhang, Y.L.; Liu, D.; Shen, Z.D.; Ding, B.; Zhang, G.B. Development of a preparation system for the radiocarbon analysis of organic carbon in carbonaceous aerosols in China. *Nucl. Instrum. Methods Phys. Res. Sect. B Beam Interact. Mater. At.* **2010**, *268*, 2831–2834. [CrossRef]
2. Wan, Z.C.; Song, K.; Zhu, W.F.; Yu, Y.; Wang, H.; Shen, R.Z.; Tan, R.; Lv, D.Q.; Gong, Y.Z.; Yu, X.N.; et al. A Closure Study of Secondary Organic Aerosol Estimation at an Urban Site of Yangtze River Delta, China. *Atmosphere* **2022**, *13*, 1679. [CrossRef]
3. Li, X.R.; Wang, Y.F.; Guo, X.Q.; Wang, Y.S. Size Distribution and Characteristics of EC and OC in Aerosols During the Olympics of Beijing, China. *Environ. Sci.* **2011**, *32*, 313–318.
4. Niu, Z.C.; Zhang, F.W.; Kong, X.R.; Chen, J.S.; Yin, L.Q.; Xu, L.L. One-year measurement of organic and elemental carbon in size-segregated atmospheric aerosol at a coastal and suburban site in Southeast China. *J. Environ. Monit. JEM* **2012**, *14*, 2961–2967. [CrossRef] [PubMed]
5. Shangping, J.; Litao, W.; Le, Z.; Qi, M.Y.; Lu, X.H.; Wang, Y.; Liu, Z.T.; Tan, J.Y.; Liu, Y.Y.; Du, C. Concentrations, sources and changes of carbon fractions in $PM_{2.5}$ in Handan. *J. Environ. Sci.* **2019**, *39*, 2873–2880.
6. Srinivas, B.; Sarin, M.M. $PM_{2.5}$, EC and OC in atmospheric outflow from the Indo-Gangetic Plain: Temporal variability and aerosol organic carbon-to-organic mass conversion factor. *Sci. Total Environ.* **2014**, *487*, 196–205. [CrossRef]
7. He, K.B.; Yang, F.M.; Ma, Y.L.; Zhang, Q.; Yao, X.H.; Chan, C.K.; Cadle, S.; Chan, T.; Mulawa, P. The characteristics of $PM_{2.5}$ in Beijing, China. *Atmos. Environ.* **2001**, *35*, 4959–4970. [CrossRef]
8. Juda-Rezler, K.; Reizer, M.; Maciejewska, K.; Blaszczak, B.; Klejnowski, K. Characterization of atmospheric $PM_{2.5}$ sources at a Central European urban background site. *Sci. Total Environ.* **2020**, *713*, 136729. [CrossRef] [PubMed]
9. Liu, S.; Ma, T.; Yang, Y.; Gao, J.; Peng, L. Chemical Composition Characteristic and Source Apportionment of $PM_{2.5}$ during Winter in Taiyuan. *Environ. Sci.* **2019**, *40*, 1537–1544.
10. Zou, C.W.; Wang, J.Y.; Hu, K.Y.; Li, J.L.; Yu, C.L.; Zhu, F.X.; Huang, H. Distribution Characteristics and Source Apportionment of Winter Carbonaceous Aerosols in a Rural Area in Shandong, China. *Atmosphere* **2022**, *13*, 1858. [CrossRef]

11. Shen, S.; Liu, L.; Wen, W.; Xing, Y.; Su, W.; Sun, J.Q. Pollution characterization and source analysis of carbon components of $PM_{2.5}$ in Beijing and surrounding areas in summer. *Environ. Eng.* **2022**, *40*, 71–80.
12. Zhang, L.B.; Sun, P.; Luo, S.N. Characteristics and Sources Analysis of Organic Carbon and Elemental Carbon Pollutionin in PM_{10} in Harbin City. *Environ. Sci. Manag.* **2020**, *45*, 130–133.
13. Li, Z.; Li, J.; Wang, S.; Zheng, X.B.; Qu, J. Characteristics and Sources Analysis of Organic Carbon and Elemental Carbon in PM_{10} in Shenyang City. *Environ. Sci. Manag.* **2020**, *45*, 113–117.
14. Pei, Y.X.; Wang, H.L.; Tan, Y.; Zhu, B.; Zhao, T.L.; Lu, W.; Shi, S.S. Analysis of BC Pollution Characteristics under $PM_{2.5}$ and O_3 Pollution Conditions in Nanjing from 2015 to 2020. *Atmosphere* **2022**, *13*, 1440. [CrossRef]
15. Huang, H.; Zou, C.W.; Cao, J.J.; PoKeung, T. Carbonaceous Aerosol Characteristics in Outdoor and Indoor Environments of Nanchang, China, during Summer. *Air Waste Manag. Assoc.* **2009**, *61*, 1262–1272. [CrossRef] [PubMed]
16. Zou, C.W.; Zhang, Y.K.; Gao, Y.T.; Mao, X.Y.; Huang, H.; Tan, Y.L. Characteristics, distribution, and sources of particulate carbon in rainfall collected by a sequential sampler in Nanchang, China. *Atmos. Environ.* **2020**, *235*, 117619. [CrossRef]
17. Huang, H.; Zou, C.W.; Cao, J.J.; PoKeung, T.; Zhu, F.X.; Yu, C.L.; Xue, S.J. Water-soluble Ions in $PM_{2.5}$ on the Qianhu Campus of Nanchang University, Nanchang City: Indoor-Outdoor Distribution and Source Implications. *Aerosol Air Qual. Res.* **2012**, *12*, 435–443. [CrossRef]
18. Chang, Q. Study on the Distribution Characteristics of Organic and Elemental Carbon in Atmospheric Particles in Shijiazhuang City. Master's Thesis, Hebei University of Science and Technology, Shijiazhuang, China, 2015. [CrossRef]
19. Shen, Y.; Liu, J.G.; Lu, V.; Ding, Q.; Shi, J.G. Comparative of Thermal-Optical Transmission and Thermal-Optical Reflectance Methods of Measurement of Organic and Elemental Carbon in Atmospheric Aerosol. *J. Atmos. Environ. Opt.* **2011**, *6*, 450–456.
20. Wang, Y.J.; Dong, Y.P.; Feng, J.L.; Guan, J.J.; Zhao, W.; Li, H.J. Characteristics and influencing factors of carbon-containing substances in $PM_{2.5}$ in Shanghai. *Environ. Sci.* **2010**, *31*, 1755–1761.
21. Li, R.; Wang, J.; Xue, K.X.; Fang, C.S. Spatial and temporal distribution characteristics and influencing factors analysis of particulate matter pollution in Jinan City. *Air Qual. Atmos. Health* **2021**, *14*, 1267–1278. [CrossRef]
22. He, Q.; Guo, Q.H.; Umeki, K.; Ding, L.; Wang, F.C.; Yu, G.S. Soot formation during biomass gasification: A critical review. *Renew. Sustain. Energy Rev.* **2021**, *139*, 110710. [CrossRef]
23. Xue, F.L.; Niu, H.Y.; Wu, Z.X.; Ren, X.L.; Li, S.J.; Wang, J.X.; Yue, L.; Fan, J.S. Pollution characteristics of organic and elemental carbon in $PM_{2.5}$ and PM_{10} in Handan City. *Environ. Chem.* **2021**, *40*, 3246–3257.
24. Dong, G.M.; Tang, G.Q.; Zhang, J.K.; Liu, Q.; Yan, G.X.; Cheng, M.T.; Wenkang, G.; Yinghong, W. Characterization of carbonaceous fraction in $PM_{2.5}$ in southern Beijing city. *Environ. Sci.* **2020**, *41*, 4374–4381.
25. Liu, J.J.; Hu, X.Z.; Huang, F.L.; Luo, Y.; Ma, S.X. Pollution characteristics of organic and elemental carbon in $PM_{2.5}$ in Guangzhou. *J. Hunan Univ. Sci. Technol. (Nat. Sci. Ed.)* **2019**, *34*, 111–117.
26. Li, Z.; Li, J.; Wang, S.; Han, Y.Y.; Qu, J. Characteristics and source analysis of organic and elemental carbon pollution in $PM_{2.5}$ in Shenyang city in spring and summer. *Environ. Sci. Manag.* **2019**, *44*, 100–105.
27. Zhao, M.F.; Qiao, T.; Huang, Z.S.; Zhu, M.Y.; Xu, W.; Xiu, G.L.; Tao, J.; Li, S.C. Comparison of ionic and carbonaceous compositions of $PM_{2.5}$ in 2009 and 2012 in Shanghai, China. *Sci. Total Environ.* **2015**, *536*, 695–703. [CrossRef]
28. Li, H.M.; Wang, Q.G.; Yang, M.; Li, F.Y.; Wang, J.H.; Sun, Y.X.; Wang, C.; Wu, H.F.; Qian, X. Chemical characterization and source apportionment of $PM_{2.5}$ aerosols in a megacity of Southeast China. *Atmos. Res.* **2016**, *181*, 288–299. [CrossRef]
29. Soleimanian, E.; Mousavi, A.; Taghvaee, S.; Sowlat, M.H.; Hasheminassab, S.; Polidori, A.; Sioutas, C. Spatial trends and sources of $PM_{2.5}$ organic carbon volatility fractions (OCx) across the Los Angeles Basin. *Atmos. Environ.* **2019**, *209*, 201–211. [CrossRef]
30. Maritz, P.; Beukes, J.P.; van Zyl, P.G.; Liousse, C.; Gardrat, E.; Ramandh, A.; Mkhatshwa, G.V. Temporal and source assessments of organic and elemental carbon at sites in the northern South African interior. *J. Atmos. Chem.* **2019**, *76*, 263–287. [CrossRef]
31. Jeong, C.H.; Traub, A.; Huang, A.; Hilker, N.; Wang, J.M.; Herod, D.; Dabek-Zlotorzynska, E.; Celo, V.; Evans, G.J. Long-term analysis of $PM_{2.5}$ from 2004 to 2017 in Toronto: Composition, sources, and oxidative potential. *Environ. Pollut.* **2020**, *263*, 114652. [CrossRef]
32. Kim, K.H.; Sekiguchi, K.; Furuuchi, M.; Sakamoto, K. Seasonal variation of carbonaceous and ionic components in ultrafine and fine particles in an urban area of Japan. *Atmos. Environ.* **2011**, *45*, 1581–1590. [CrossRef]
33. Yu, G.H.; Park, S. Chemical characterization and source apportionment of $PM_{2.5}$ at an urban site in Gwangju, Korea. *Atmos. Pollut. Res.* **2021**, *12*, 101092. [CrossRef]
34. Sandeep, K.; Negi, R.S.; Panicker, A.S.; Gautam, A.S.; Bhist, D.S.; Beig, G.; Murthy, B.S.; Latha, R.; Singh, S.; Das, S. Characteristics and Variability of Carbonaceous Aerosols over a Semi Urban Location in Garhwal Himalayas. *Asia-Pac. J. Atmos. Sci.* **2019**, *56*, 455–465. [CrossRef]
35. Chow, J.C.; Watson, J.G.; Zhiqiang, L.; Lowenthal, D.H.; Frazier, C.A.; Solomon, P.A.; Thuillier, R.H.; Magliano, K. Descriptive analysis of $PM_{2.5}$ and PM_{10} at regionally representative locations during SJVAQS/AUSPEX. *Atmos. Environ.* **1996**, *30*, 2079–2112. [CrossRef]
36. Cao, J.J.; Wu, F.; Zhou, J.C.; Li, S.C.; Li, Y.H.; Chen, S.H.; An, Z.S.; Feng, G.Q.; Watson, J.G.; Zhu, C.S.; et al. Characterization and source apportionment of atmospheric organic and elemental carbon during fall and winter of 2003 in Xi'an, China. *Atmos. Chem. Phys.* **2005**, *5*, 3127–3137. [CrossRef]
37. Zhang, W.J.; Li, M.; Fu, H.X.; Ge, X.; Lv, B.; Wang, Z.F.; Li, H.B. Analysis of $PM_{2.5}$ chemical components and pollution characteristics in Jinan. *Environ. Pollut. Prev.* **2019**, *41*, 1490–1494.

38. Turpin, B.J.; Huntzicker, J.J. Identification of secondary organic aerosol episodes and quantitation of primary and secondary organic aerosol concentrations during SCAQS. *Atmos. Environ.* **1995**, *29*, 3527–3544. [CrossRef]
39. Pio, C.; Cerqueira, M.; Roy, M.; Harrison, R.M.; Nunes, T.; Mirante, F.; Alves, C.; Oliveira, C.; Campa, A.S.; Artíñano, B.; et al. OC/EC ratio observations in Europe: Re-thinking the approach for apportionment between primary and secondary organic carbon. *Atmos. Environ.* **2020**, *235*, 117619. [CrossRef]
40. Chen, Y.J.; Zhi, G.R.; Feng, Y.L.; Fu, J.M.; Feng, J.L.; Sheng, G.Y. Measurements of emission factors for primary carbonaceous particles from residential raw-coal combustion in China. *Geophys. Res. Lett.* **2006**, *33*. [CrossRef]
41. Han, Y.M.; Cao, J.J.; Li, S.C.; He, G.F.; An, Z.S. Different characteristics of char and soot in the atmosphere and their ratio as an indicator for source identification in Xi'an, China. *Atmos. Chem. Phys.* **2010**, *10*, 595–607. [CrossRef]
42. Chow, J.C.; Watson, J.G.; Kuhns, H.; Etyemezian, V.; Lowenthal, D.H.; Crow, D.; Kohl, S.D.; Engelbrecht, J.P.; Green, M.C. Source profiles for industrial, mobile, and area sources in the Big Bend Regional Aerosol Visibility and Observational study. *Chemosphere* **2004**, *54*, 185–208. [CrossRef] [PubMed]
43. Feng, J.L.; Yu, H.; Su, X.F.; Liu, S.H.; Li, Y.; Pan, Y.P.; Sun, J.H. Chemical composition and source apportionment of $PM_{2.5}$ during Chinese Spring Festival at Xinxiang, a heavily polluted city in North China: Fireworks and health risks. *Atmos. Res.* **2016**, *182*, 176–188. [CrossRef]
44. Li, X.H.; Wang, S.X.; Duan, L.; Hao, J.M.; Li, C.; Chen, Y.S.; Yang, L. Particulate and trace gas emissions from open burning of wheat straw and corn stover in China. *Environ. Sci. Technol.* **2007**, *41*, 6052–6058. [CrossRef] [PubMed]
45. Jia, X.H.; Xie, J.F.; Ma, X.; Di, Z.D.; Wu, Y.N. Analysis of water-soluble constituents in winter of $PM_{2.5}$ in Taiyuan city. *China Environ. Sci.* **2013**, *33*, 599–604.